

Article

Core/Shell Glycine-Polyvinyl Alcohol/Polycaprolactone Nanofibrous Membrane Intended for Guided Bone Regeneration: Development and Characterization

Marwa Alazzawi ¹, Nabeel Kadim Abid Alsahib ¹ and Hilal Turkoglu Sasmazel ^{2,*} 

¹ Department of Biomedical Engineering, Al Nahrain University, Al Jadriya Bridge, Baghdad 64074, Iraq; marwa.azzawi86@gmail.com (M.A.); n_k_alsahib@yahoo.com (N.K.A.A.)

² Department of Metallurgical and Materials Engineering, Atilim University, Incek, 06830 Golbasi, Turkey

* Correspondence: hilal.sasmazel@atilim.edu.tr

Abstract: Glycine (Gly), which is the simplest amino acid, induces the inflammation response and enhances bone mass density, and particularly its β polymorph has superior mechanical and piezoelectric properties. Therefore, electrospinning of Gly with any polymer, including polyvinyl alcohol (PVA), has a great potential in biomedical applications, such as guided bone regeneration (GBR) application. However, their application is limited due to a fast degradation rate and undesirable mechanical and physical properties. Therefore, encapsulation of Gly and PVA fiber within a poly(ϵ -caprolactone) (PCL) shell provides a slower degradation rate and improves the mechanical, chemical, and physical properties. A membrane intended for GBR application is a barrier membrane used to guide alveolar bone regeneration by preventing fast-proliferating cells from growing into the bone defect site. In the present work, a core/shell nanofibrous membrane, composed of PCL as shell and PVA:Gly as core, was developed utilizing the coaxial electrospinning technique and characterized morphologically, mechanically, physically, chemically, and thermally. Moreover, the characterization results of the core/shell membrane were compared to monolithic electrospun PCL, PVA, and PVA:Gly fibrous membranes. The results showed that the core-shell membrane appears to be a good candidate for GBR application with a nano-scale fiber of 412 ± 82 nm and microscale pore size of 6.803 ± 0.035 μ m. Moreover, the wettability of $47.4 \pm 2.2^\circ$ contact angle (C.A) and mechanical properties of 135 ± 3.05 MPa average modulus of elasticity, 4.57 ± 0.04 MPa average ultimate tensile stress (UTS), and $39.43\% \pm 0.58\%$ average elongation at break are desirable and suitable for GBR application. Furthermore, the X-ray diffraction (XRD) and transmission electron microscopy (TEM) results exhibited the formation of β -Gly.

Keywords: glycine; GBR; coaxial; core-shell; electrospinning; encapsulation



Citation: Alazzawi, M.; Kadim Abid Alsahib, N.; Turkoglu Sasmazel, H. Core/Shell Glycine-Polyvinyl Alcohol/Polycaprolactone Nanofibrous Membrane Intended for Guided Bone Regeneration: Development and Characterization. *Coatings* **2021**, *11*, 1130. <https://doi.org/10.3390/coatings11091130>

Academic Editor: Anton Fica

Received: 29 August 2021

Accepted: 13 September 2021

Published: 17 September 2021

Publisher's Note: MDPI stays neutral with regard to jurisdictional claims in published maps and institutional affiliations.



Copyright: © 2021 by the authors. Licensee MDPI, Basel, Switzerland. This article is an open access article distributed under the terms and conditions of the Creative Commons Attribution (CC BY) license (<https://creativecommons.org/licenses/by/4.0/>).

1. Introduction

During the last decade, biomaterial science has become an essential field in tissue regeneration applications. The main goal of tissue regeneration application is to promote cells attachment, proliferation, differentiation, and migration through a scaffold that mimics the natural extracellular matrix (ECM) [1,2]. GBR is one of the strategies that have been applied to restore the lost alveolar bone and obtain proper integration and support during the functional loading of an implant. Several systematic and periodontal diseases, which cause bone loss or insufficiency, in addition to trauma and tumors, are the main concerns for osseointegration. In order to achieve long-term and stable implantation, a sufficient volume of bone should exist at the implantation area [3]. Therefore, the GBR membrane achieves its goal when the osteoprogenitor cells are exclusively allowed to grow in the bone defect by preventing the entry of non-osteogenic tissue. Furthermore, the ideal membrane for GBR should be biocompatible, mechanically suitable, cell occlusive, host tissue integration, and clinically manageable. Anti-inflammatory and bone regeneration

enhancement are additional properties that improve GBR function [4]. Electrospinning has become one of the most studied fabrication techniques in tissue regeneration application due to its affordability, versatility, cost-effectivity, and adaptability [5–7]. The fabricated nano/microscale fibrous scaffolds provide support for tissue regeneration and promote cell attachment, proliferation, and migration [5]. However, the dense packing of fibers generates small pore sizes, which obstructs cell infiltration and limits its use in some tissue regeneration applications, although it is useful in other tissue regeneration applications, including GBR [8]. Coaxial electrospinning is a modification of the electrospinning process in which coaxially aligned needles are utilized to generate core-shell fibers. The core-shell fibers overcome the limitation of monolithic electrospun fibers, including degradability, bioactivity, and inappropriate mechanical properties, in addition to burst release of the incorporating molecules [9,10].

A variety of materials have been studied and utilized in manufacturing GBR membranes; generally, they are roughly divided into bioresorbable and non-resorbable membranes. Non-resorbable membrane materials include polytetrafluoroethylene (e-PTFE), high-density polytetrafluoroethylene (d-PTFE), and titanium-reinforced high-density polytetrafluoroethylene (Ti-d-PTFE) [11]. The main advantage of non-resorbable membranes is good space-maintaining, while disadvantages are the need for a second surgery to be removed due to non-resorbability, stiff to handle, and insufficient healing of soft tissue due to tension and lack of vascular supply, which leads to membrane exposure with subsequent progression of infection [12]. On the other hand, a bioresorbable membrane was introduced in order to avoid a second surgical operation. The commercial bioresorbable GBR membranes that are made from mainly of synthetic polymers, including poly (lactic acid) (PLA), Poly (glycolic acid) (PGA), and PCL, and their copolymers and composites [13]. However, the main challenges of bioresorbable GBR membranes are inappropriate mechanical properties, short resorption period, usually in the range of four to six months, and side effects of their degradation by-products on bone formation [14].

In this paper, a core-shell fibrous structure was fabricated using coaxial electrospinning, in which the PCL is the shell and PVA with Gly is the core. The Gly has an anti-inflammatory response [15] and enhances bone mass density [16], and particularly its β polymorph has superior mechanical [17] and piezoelectric properties [18–20]. On the other hand, PCL and PVA, which are FDA-approved bioresorbable synthetic polymers, were utilized in membrane fabrication due to their biodegradability with non-toxic by-products (mainly CO_2 and H_2O), biocompatibility, good tensile strength, and processability [21,22]. However, the rapid degradation rate with high shrinkage and absorption percentage and undesirable mechanical properties of the monolithic electrospun membrane act as limitations in using these materials in membrane fabrication. Therefore, PCL was used to encapsulate the PVA and Gly fiber in core-shell nanofibers in order to preserve the Gly in its β polymorph form and to overcome the limitation of monolithic electrospun Gly with PVA. Moreover, the necessity of a cross-linking step for Gly with PVA electrospun membrane is discarded due to encapsulation with PCL that has a longer degradation rate. Consequently, the novelty of this paper mainly is the inclusion of β -Gly in GBR membrane fabrication according to its stated advantages and the fiber structure of the fabricated membrane, which was encapsulated with PCL that preserves the Gly with the PVA inside.

The main aim of this paper is to develop and characterize a coaxially electrospun core-shell fibrous membrane made of Gly and PVA as the core materials and PCL as the shell material for GBR application. In order to pursue the aim of the paper, four different membranes were optimized and electrospun utilizing coaxial and single electrospinning processes. The membranes were characterized morphologically, chemically, physically, mechanically, and thermally. The morphology of the four membranes was characterized using scanning electron microscopy (SEM), and the core-shell structure was investigated using transmission electron microscopy (TEM). The chemical composition of the membranes was characterized using X-ray spectroscopy (XPS); in addition, the crystallographic structure of the Gly in the PVA:Gly and core-shell membranes was determined using X-ray diffraction

(XRD) analysis. Moreover, the mechanical properties were obtained using tensile testing and the thermal and physical properties were acquired using thermal gravimetric analysis (TGA), C.A analysis, in vitro degradation analysis, and absorption and shrinkage tests.

2. Materials and Methods

2.1. Materials

In order to prepare the fibrous membranes, PVA with $M_w = 85,000\text{--}124,000$ g/mol and +99% hydrolyzed, and PCL, which is linear, and with $M_w = 80,000$ g/mol, were purchased from Sigma-Aldrich (St. Louis, MO, USA). The Gly was purchased from ISOLAB Laborgeräte GmbH (Eschau, Germany) in the form of white powder and was more than 99% pure, in addition to the chloroform and methanol, which were used for solution preparation. Phosphate buffer saline (PBS) was obtained from Amresco (Solon, OH, USA), and Triton-X 100 was purchased as a 10% (*w/v*) aqueous solution from Sigma-Aldrich (Taufkirchen, Germany). Pure water and ultra-pure water used in solution preparation and wettability measurements were attained in the laboratory using a water purification system (New Human Power III, Human, Seoul, Korea) and the reverse osmosis technique.

2.2. Experimental

2.2.1. Preparation and Electrospinning of Membranes

Four different membranes were optimized and fabricated using the electrospinning process. In order to prepare the first membrane solution, PCL was dissolved in a chloroform/methanol 5/1 (*v/v*) mixture to give a concentration of 5% (*w/v*). The PCL solution was stirred using a magnetic stirrer (Daihan wisd, Seoul, Korea) at room temperature for three hours until completely dissolved. On the other hand, the PVA membrane was prepared by dissolving the PVA in pure water at the concentration of 8% (*w/v*) at 80–85 °C for 3 to 4 h until complete dissolution was observed, then after cooling down, 0.5 mL of Triton X-100 was added and magnetically stirred with the PVA solution for half an hour. While PVA and Gly were dissolved in pure water at the concentration of 8% (*w/v*) with 4:1 PVA to Gly weight ratio, the weight percentage content of the Gly is 20% of the PVA matrix, at 80–85 °C until complete dissolution was observed by naked-eye, the dissolution process took almost 3 to 4 h, thereafter 0.5 mL of Triton X-100 was added to the solution and stirred. The fourth membrane, which is the core-shell membrane, was prepared by dissolving PCL in chloroform/methanol 5/1 volume ratio mixture for the shell layer solution preparation and dissolving PVA and Gly at a 4:1 weight ratio to give 8% (*w/v*) concentration for the core solution preparation. Both core and shell solutions were prepared using the same preparation process as the PCL and PVA:Gly membranes mentioned above.

Thereafter, the prepared solutions were placed into a 5 mL syringe, and a polyethylene tube with a metal needle end was used to electrospin the monolithic electrospun membranes. While in core-shell membrane electrospinning, the core and the shell solutions were placed in different syringes, and each syringe was connected to the coaxial needle (Inovenso, Istanbul, Turkey) through a polyethylene tube, as shown in Figure 1b. The coaxial needle with 0.8 mm inner diameter for core needle and 1.6 mm inner diameter for shell needle was utilized for core-shell membrane electrospinning. While a 21-gauge needle was used for monolithic membrane electrospinning. Moreover, each syringe was placed in an infusion pump (SKE research equipment, Milan, Italy) in order to control the feeding rate, and a commercial electrospinning apparatus (Inovenso NE-200, Istanbul, Turkey), which is shown in Figure 1a, was used for electrospinning the membranes. Furthermore, the electrospinning parameters were optimized and listed in Table 1.

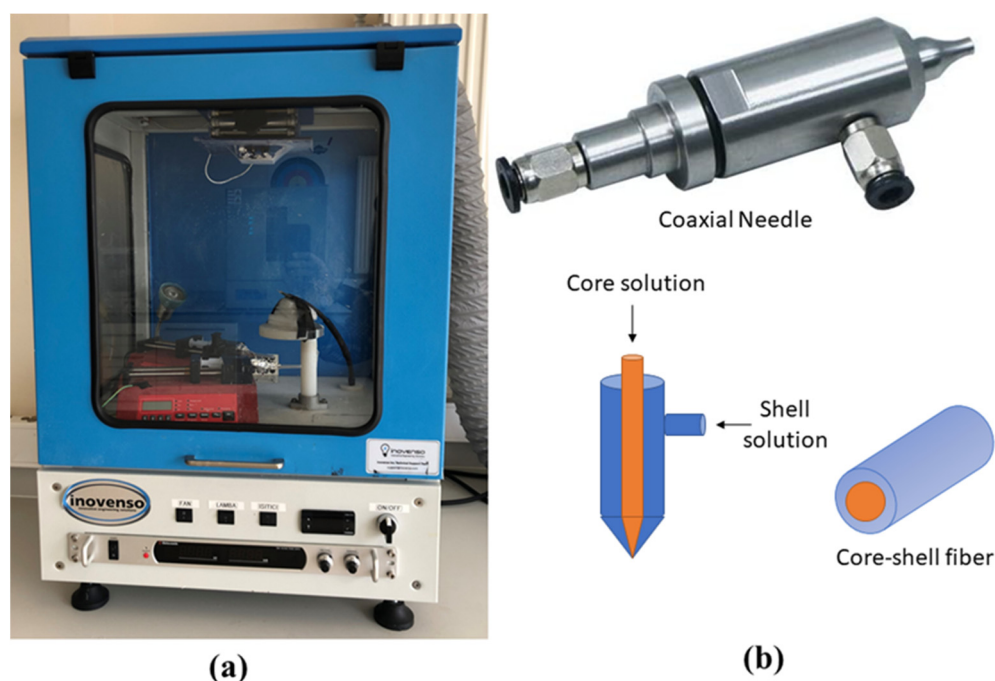


Figure 1. (a) Electrospinning device used for membrane fabrication; (b) coaxial electrospinning needle and core-shell fiber structure.

Table 1. Electrospinning parameters of the fabricated membranes.

Membrane	Applied Voltage (kV)	Needle-to-Collector Distance (cm)	Feeding Rate ($\mu\text{L}/\text{min}$)
PCL	7	10	10
PVA	17	15	10
PVA:Gly	11.5	15	10
Core-shell	20	22	Core: 27 Shell: 20

The fabricated membranes were reserved in a porcelain desiccator from Sigma-Aldrich (Taufkirchen, Germany) for three days before any further characterization. Thereafter, the membranes were weighted, and the average weight of the membranes was calculated. The macroscopic image of the prepared membrane as shown in Figure 2a. The physical state of the core-shell membrane is also shown in different macroscopic views in Figure 2b.

2.2.2. Characterization

Four membranes were characterized morphologically, chemically, mechanically, thermally, and physically as follows:

- SEM analysis.

In order to examine the fabricated membranes morphology and find the fiber diameter and pore size, an SEM device (Zeiss EVO 15LS, Jena, Germany) was utilized. Membranes were cut into small pieces and mounted on an aluminum stub using double-sided conductive adhesive tape, and then the specimens were sputter-coated with a gold-palladium thin coat. The average fiber diameter and pore size was calculated from the obtained SEM micrographs via ImageJ Launcher open-source software program, and the average of at least 50 measurements were calculated to find fiber diameter, whereas the average of 20 measurements were calculated to find the pore size for each membrane.

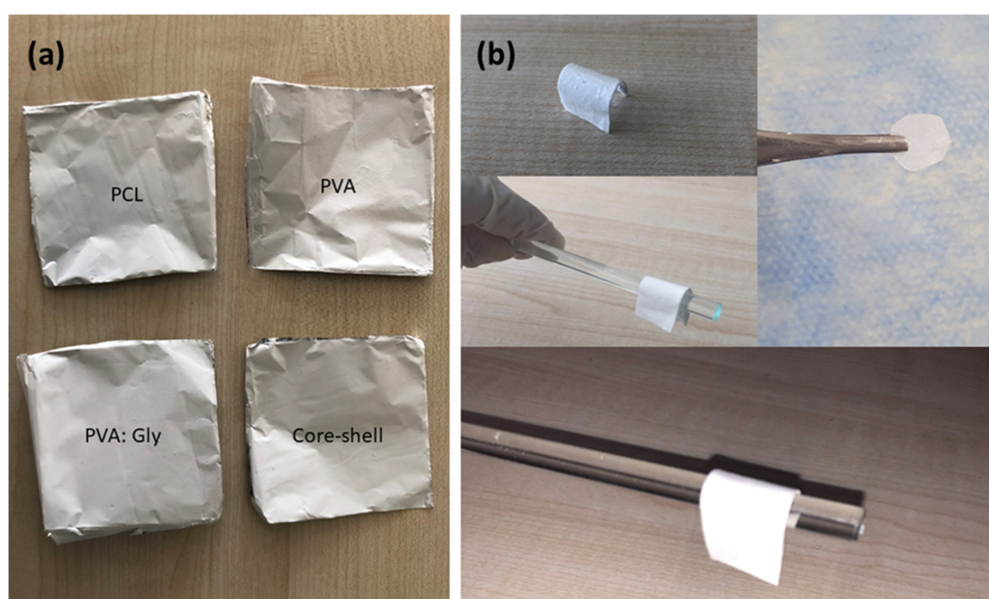


Figure 2. (a) Macroscopic images of the prepared membranes; (b) Core-shell membrane bending, space making and different macroscopic views.

- TEM analysis.

The core-shell structure was investigated using high-contrast (FEI Tecnai G2 Spirit BioTwin CTEM, FEI Company, Hillsboro, OR, USA). The samples were prepared by electrospinning a very thin layer directly onto the carbon-coated copper grid. The grids were directly used for TEM characterization without any staining.

- Tensile test.

In this paper, the mechanical properties of the fabricated membranes are particularly important. The ideal GBR membrane should have sufficient plasticity to withstand the compression of the overlying soft tissue, in addition, to be easily modified into the defect shape. On the other hand, the membrane should have a degree of tensile strength and stiffness for clinical manageability [23]. Therefore, mechanical properties of the fabricated membranes were determined following international standardization and using a universal tensile testing apparatus (Zwisch/Roell, Ulm, Germany) with 100 N load cell and a crosshead speed of 10 mm/min with a gauge length of 20 mm. All fabricated membranes were cut into a 40 mm × 5 mm dog-bone shape. Average UTS, modulus of elasticity, and elongation at break were determined in triplets.

- XPS analysis.

The surface chemical composition and functional O_{1s}, C_{1s}, and N_{1s} groups were determined from high-resolution scans using Al K α Monochromatic XPS (PHI 5000 VersaProbe, Physical Electronics, Chanhassen, MN, USA) at 600 W. Each peak in the high-resolution scans was deconvoluted using Origin (OriginPro 8.0, Origin Lab Inc., Northampton, MA, USA) software.

- XRD analysis.

One of the main goals of this thesis is to acquire the benefits of Gly in the β -polymorph crystal structure. In order to confirm the existence of β -Gly, a crystallographic structure of the fabricated core-shell and PVA:Gly membranes was determined using XRD (Ultima-IV, Tokyo, Japan). The XRD characterization range was 10–45 (2 θ) degrees, and the scanning step was 5 degrees/min.

- TGA.

In order to identify the thermal behavior of the fabricated membranes, the thermogravimetric analysis was performed using a PyrisTM 1 TGA device (PerkinElmer, Waltham,

MA, USA). The TGA traces were in the range of 25–700 °C under a nitrogen atmosphere with a heating rate of 10 °C/min. The membranes were previously dried in a porcelain dissector plate for two days at room temperature. All results were plotted as temperature versus weight loss, and curves were analyzed using OriginPro 8.0 software in order to determine the thermal decomposition temperature.

- Wettability.

The wettability using water C.A was measured for each membrane from different points using a C.A goniometry Phoenix 300 (Surface electro optics, Suwon, Korea). Values were determined according to water drop images on the surface of the material.

- In vitro degradation analysis.

The PCL is a hydrophobic linear polyester with a long degradation rate [24], while PVA is a hydrophilic linear polymer with a moderate degradation rate that depends on the hydrolysis and MW of the used PVA [25]. In any tissue regeneration application, including GBR application, the degradation of the membrane should be predictable and matches the bone formation. Therefore, an in vitro degradation study was conducted in terms of the ASTM F 1635-04 method. After drying the fabricated membranes for two days in the dissector, the initial weight (W_0) was recorded using a laboratory weighing scale with 0.1 mg accuracy. This was followed by immersing the samples in 0.1 M PBS in three replicas. The samples were stored in tubes and placed into incubation at 37 ± 0.1 °C. The PBS solution was changed every three days, and the samples were discarded from PBS liquid, washed with pure water three times to remove residuals, and blotted with clean then dried in the oven for 12 h after 5, 10, 15, 20, 25, 30, 40, 50, 60, 70, 80, and 90 days of incubation. Afterward, the final weight of each sample (W_f) was recorded, and the remaining weight was calculated using the following equation:

$$\text{Remaining Weight (\%)} = \frac{W_f}{W_0} \times 100 \quad (1)$$

- Absorption and shrinkage tests.

In any tissue supporting application, the scaffolds should resist volume and shape changes in the fluidic environment because the huge difference in volume can cause either pressure on the healing cells and cause deterioration in the healing process or insufficient healing process due to loss of support. Therefore, absorption and shrinkage tests were carried out in PBS solution for 24 h. Initially, the samples were cut into 10 mm × 10 mm square shapes and weighed accurately to be placed in tubes filled with PBS and stored in an incubator at 37.0 ± 0.1 °C. At least three measurements were obtained for each sample, and the average values and corresponding standard deviations were determined. After the incubation period, which was 24 h, the samples were removed from PBS and blotted with a clean paper towel to absorb the residual water. Finally, the samples' weights were measured, and absorption (%) was calculated according to the following equation:

$$\text{Absorption (\%)} = \frac{W_f - W_i}{W_i} \times 100 \quad (2)$$

where W_f and W_i are the weights of the samples at the end and beginning of the incubation period, respectively.

In the case of the shrinkage test, each sample was dried for 12 h after 24 h of incubation in the drying oven. Thereafter, the surface areas of the samples were determined using a micrometer before and after the drying process, and the average shrinkage (%) of three different measurements was measured according to the following formula:

$$\text{Shrinkage (\%)} = \frac{A_i - A_f}{A_i} \times 100 \quad (3)$$

where A_i was the initial area of the sample at the beginning of the incubation and A_f was the final area after drying.

- Statistical analysis.

The results were expressed as mean \pm standard deviation in experiments. Statistical analysis was performed using OriginPro 8.0 software. One-way analysis of variance (ANOVA) with statistical significance less than 0.05 significance was performed, while pairwise comparisons were conducted using Student's t -test.

3. Results

3.1. Morphological and Structural Characterization

The SEM images of the fabricated membranes shown in Figure 3 indicate a uniform, non-beaded fibrous network with interconnected porosity, which is an indication of a successful electrospinning of the prepared solutions. Moreover, using the ImageJ launcher program with the SEM images, the average fiber diameters and average pore size were calculated and summarized in Table 2, in addition to the bar graph distribution of the fiber diameter shown in Figure 3.

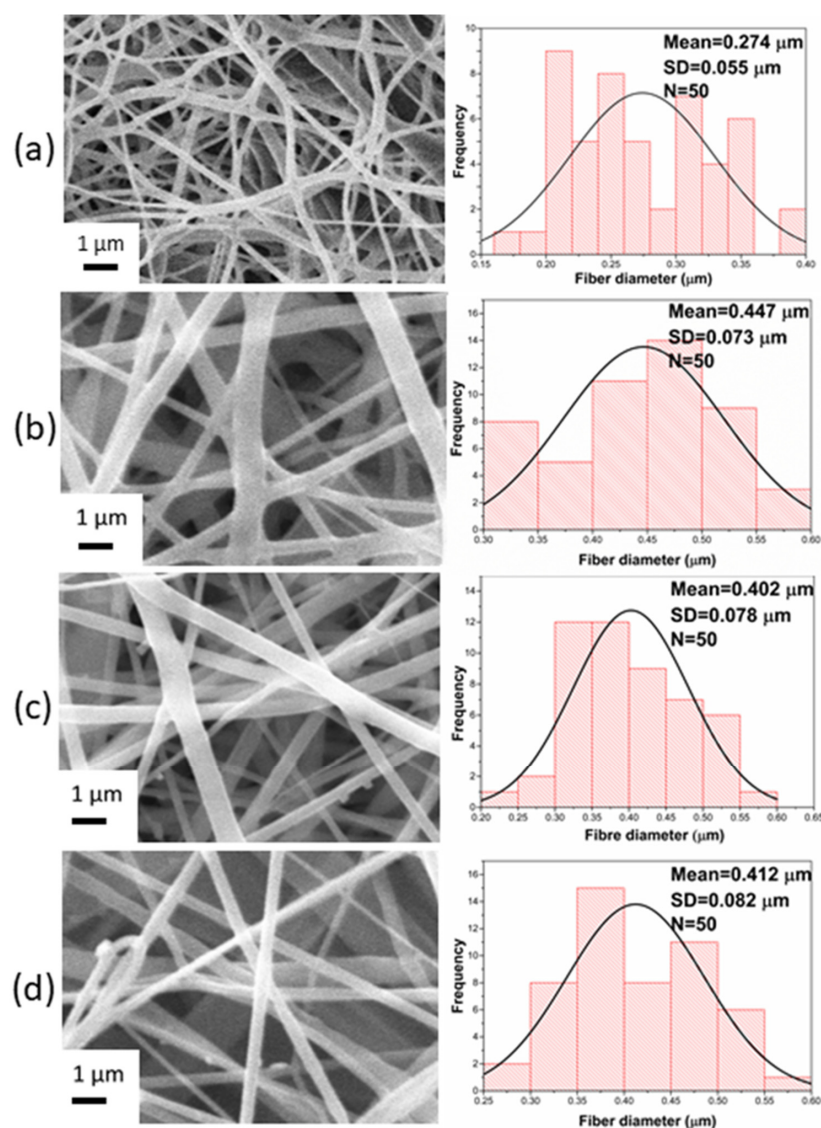
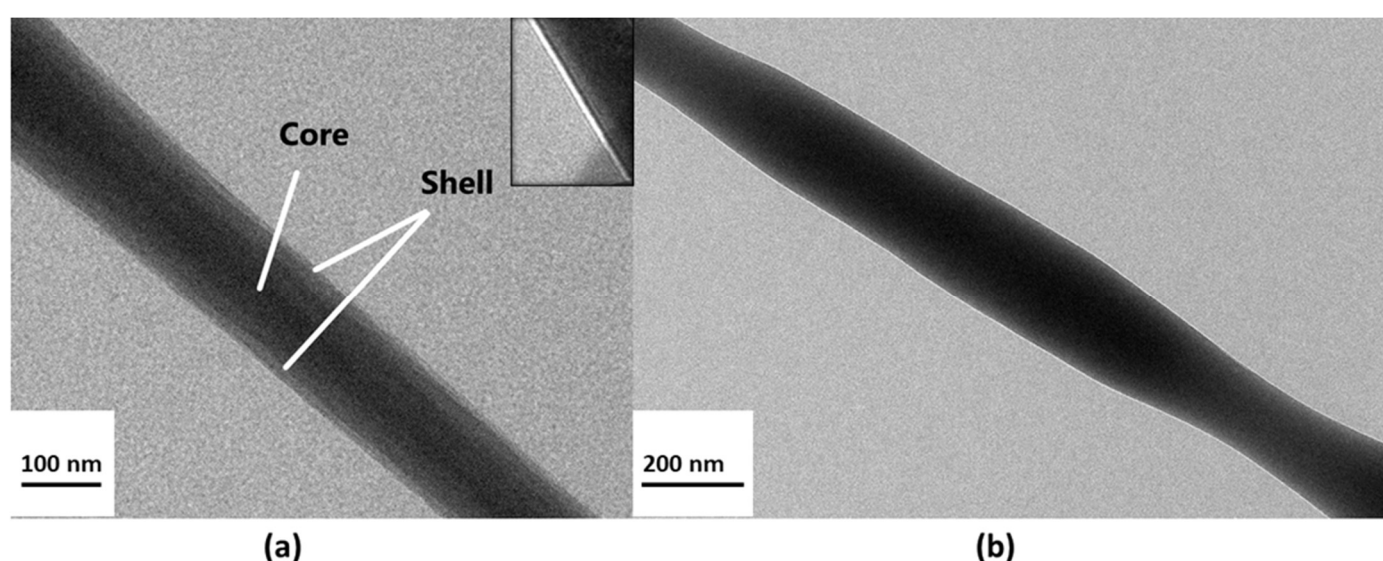


Figure 3. SEM images and bar graph of the fiber diameter distribution for the: (a) PCL; (b) PVA; (c) PVA:Gly; and (d) core-shell membranes.

Table 2. Average fiber diameter and pore size of each fabricated membrane.

Membrane	Average Fiber Diameter (μm)	Average Pore Size (μm)
PCL	0.274 ± 0.055	2.573 ± 0.016
PVA	0.447 ± 0.073	4.157 ± 0.056
PVA:Gly	0.402 ± 0.078	4.217 ± 0.103
Core-shell	0.412 ± 0.082	6.803 ± 0.035

Moreover, in order to investigate the core-shell structure, a TEM characterization was utilized to observe the core-shell formation. TEM is used to investigate the inner structure of the fibers because the electron is transmitted through a very thin specimen < 100 nm. The TEM images in Figure 4a shows the core-shell structure of the fabricated membrane with nano-scale fiber's diameter. Furthermore, the TEM images in Figure 4b show the packing of the Gly crystals inside the core-shell fibers.

**Figure 4.** TEM images of: (a) core-shell fibers and (b) Gly crystals within core-shell fiber.

3.2. Mechanical Characterization

The tensile properties of the electrospun PCL, PVA, PVA:Gly, and core-shell membranes, including modulus of elasticity, UTS, and elongation at break, are shown in Table 3.

Table 3. The average modulus of elasticity, UTS, and elongation at break of the fabricated membranes.

Membrane	Modulus of Elasticity (MPa)	Ultimate Tensile Strength (MPa)	Elongation at Break (%)
PCL	2.86 ± 0.07	4.23 ± 0.01	120 ± 3
PVA	49.7 ± 0.556	1.19 ± 0.1	11.3 ± 2.02
PVA:Gly	241.3 ± 1.52	5.69 ± 0.02	19 ± 0.98
Core-shell	135.3 ± 3.05	4.57 ± 0.04	39.43 ± 0.58

3.3. Chemical Characterization

3.3.1. XPS Characterization

A high-resolution scan of O_{1s} , C_{1s} , and N_{1s} was conducted using XPS, and spectrum peaks were deconvoluted utilizing OriginPro 8.0 software (Figure 5). The C_{1s} high resolution peaks of PCL and core-shell membranes represented three deconvoluted peaks at 285, 286.4, and 289 eV, while the PVA and PVA:Gly membranes showed only two C_{1s} peaks at 285 and 286.4 eV. On the other hand, the PVA and PVA:Gly membranes showed only one high resolution O_{1s} peak at 533 eV, while the PCL and core-shell membranes

demonstrated two O_{1s} high resolution peaks at 533 and 531.6 eV. No membrane revealed a high-resolution peak of N_{1s} except the PVA:Gly membrane (Figure 5i).

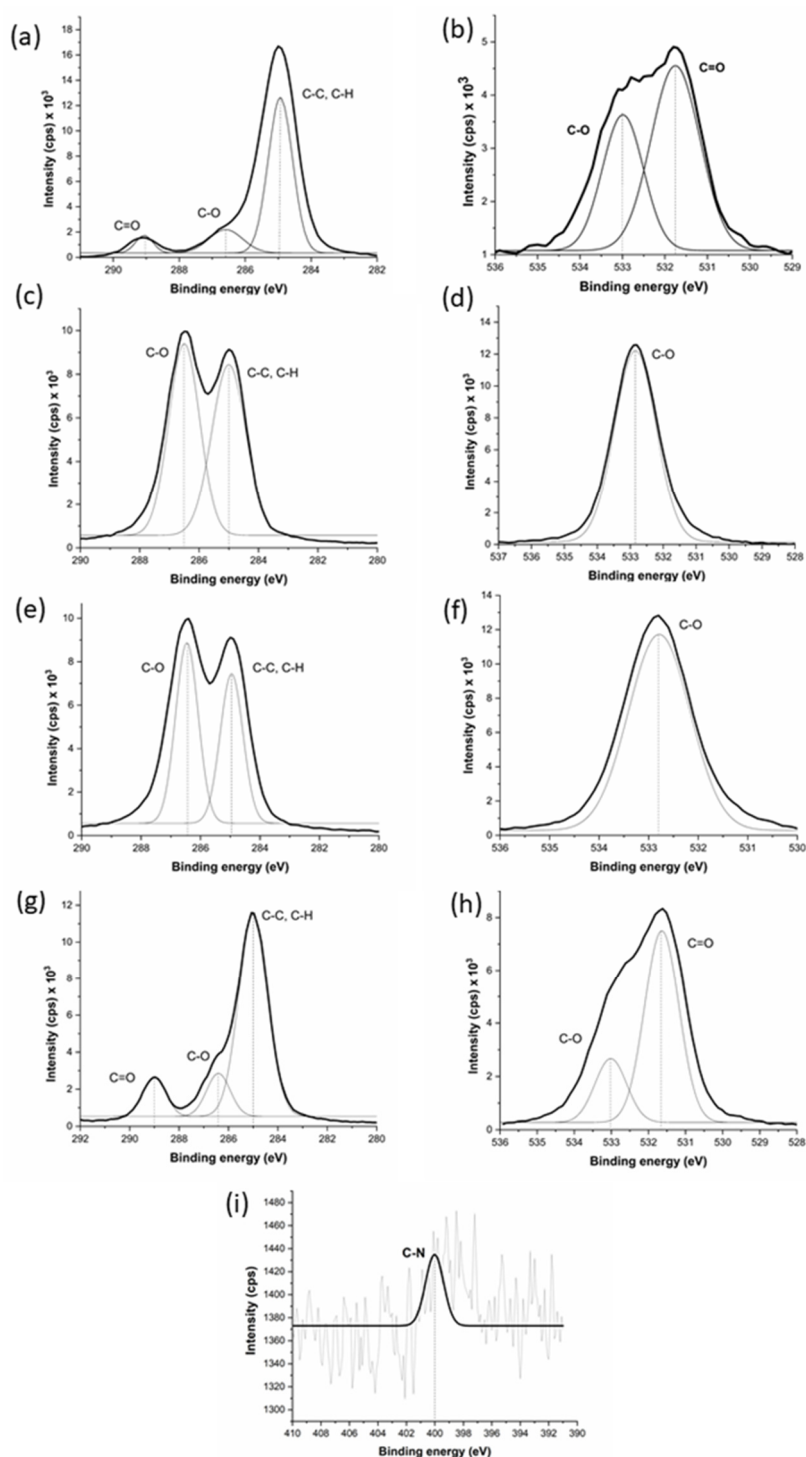


Figure 5. XPS high resolution spectra and deconvoluted peaks for: (a) PCL membrane C_{1s}; (b) PCL membrane O_{1s}; (c) PVA membrane C_{1s}; (d) PVA membrane O_{1s}; (e) PVA:Gly membrane C_{1s}; (f) PVA:Gly membrane C_{1s}; (g) core-shell membrane C_{1s}; (h) core-shell membrane C_{1s}; and (i) PVA:Gly membrane N_{1s}.

3.3.2. XRD Characterization

The XRD analysis was used to identify the β -Gly form for the PVA:Gly and core-shell membranes, and the results were plotted using OriginPro 8.0 software and demonstrated in Figure 6.

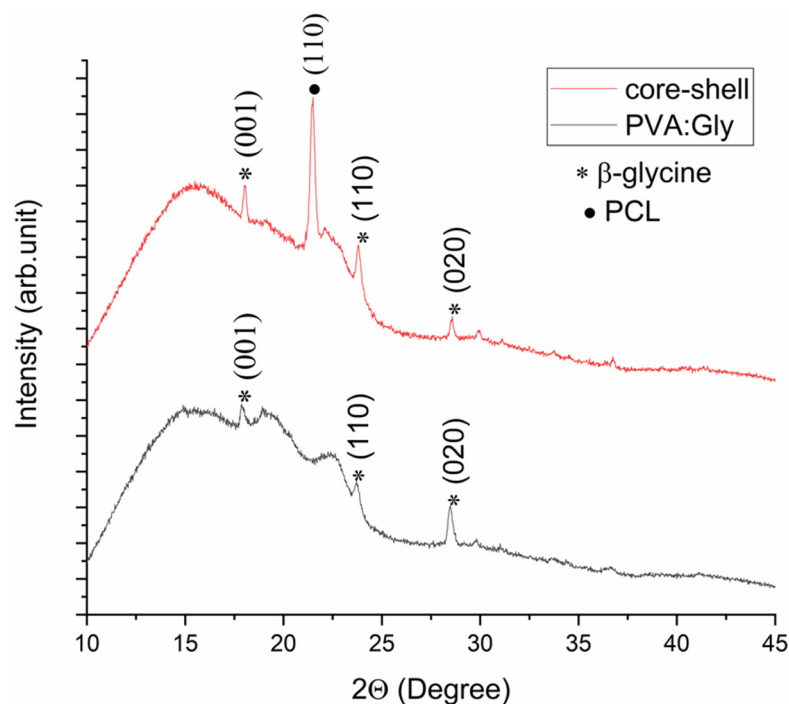


Figure 6. XRD plots of the PVA:Gly and core-shell membrane.

3.4. Thermal Characterization

In this paper, TGA was used to indicate the changes in membrane composition and thermal stability of each fabricated membrane. Figure 7 demonstrates plots that show the difference between the fabricated membranes in thermal properties using TGA.

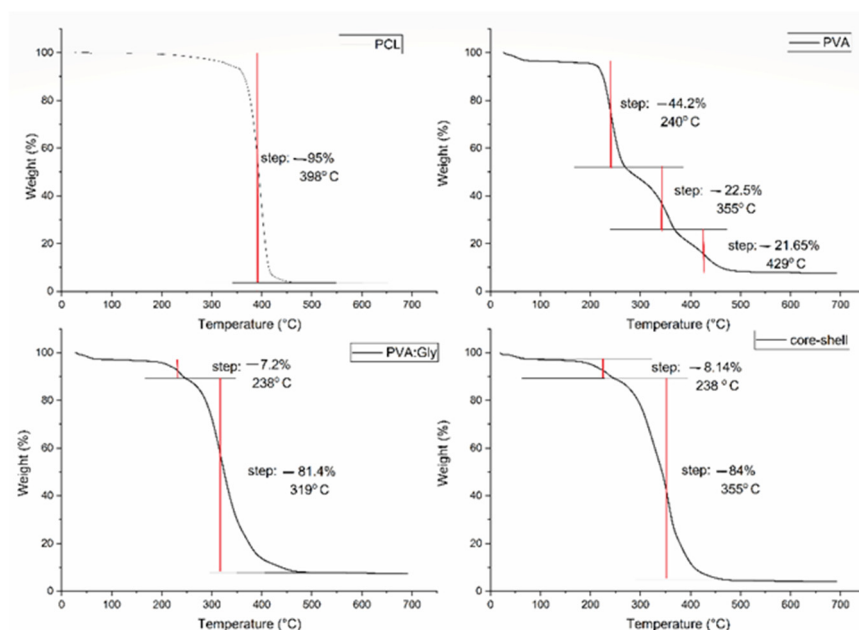


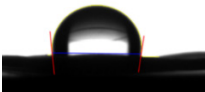



Figure 7. TGA curves of the fabricated PCL, PVA, PVA:Gly, core-shell membranes.

3.5. Physical Characterization

3.5.1. Wettability

The wettability of the fabricated membranes was assessed using the C.A method. The hydrophilicity or hydrophobicity of the fabricated membranes was determined, which is an essential parameter in material-cell interaction, depending on the C.A images and average C.A results of the fabricated membranes and were demonstrated in Table 4.

Table 4. The average contact angles and contact-angle images of the fabricated membranes.

Membranes	Average C.A	C.A Image
PCL	$100 \pm 8.1^\circ$	
PVA	~ 0	
PVA:Gly	~ 0	
Core-shell	$47.4 \pm 2.2^\circ$	

3.5.2. In Vitro Degradation

According to Figure 8, the fabricated membranes' degradation rate is represented as the average weight remaining for various intervals during 90 days of incubation period at 37°C in PBS.

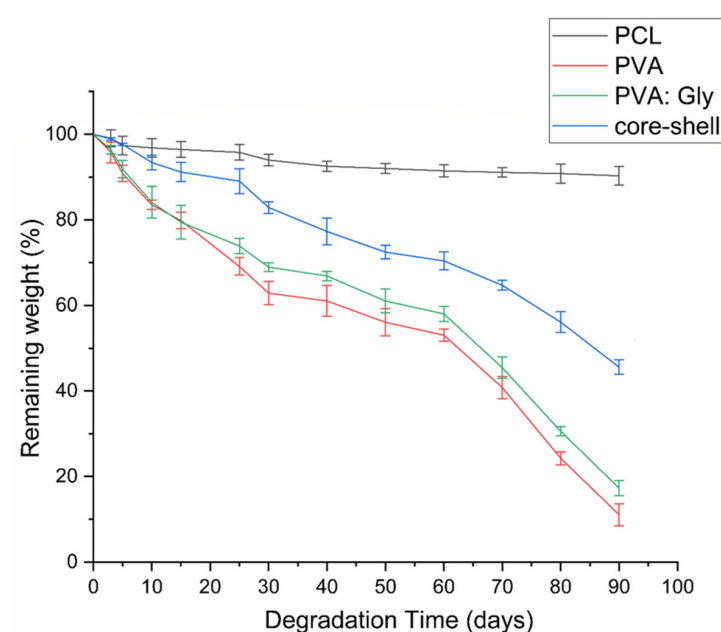


Figure 8. Remaining weight of PCL, PVA, PVA:Gly, and core-shell membranes during 90 days of incubation in PBS. All readings are presented as remaining weight% \pm standard deviation.

3.5.3. Absorption and Shrinkage Test

The average absorption % with standard deviation was calculated for each membrane, and the results were demonstrated as a bar graph in Figure 9. On the other hand, the average shrinkage % for the four fabricated membranes was found to be ~0% for PCL membrane, 95.1% for the PVA membrane, 89.4% for the PVA:Gly membrane, and ~1% for the core-shell membrane.

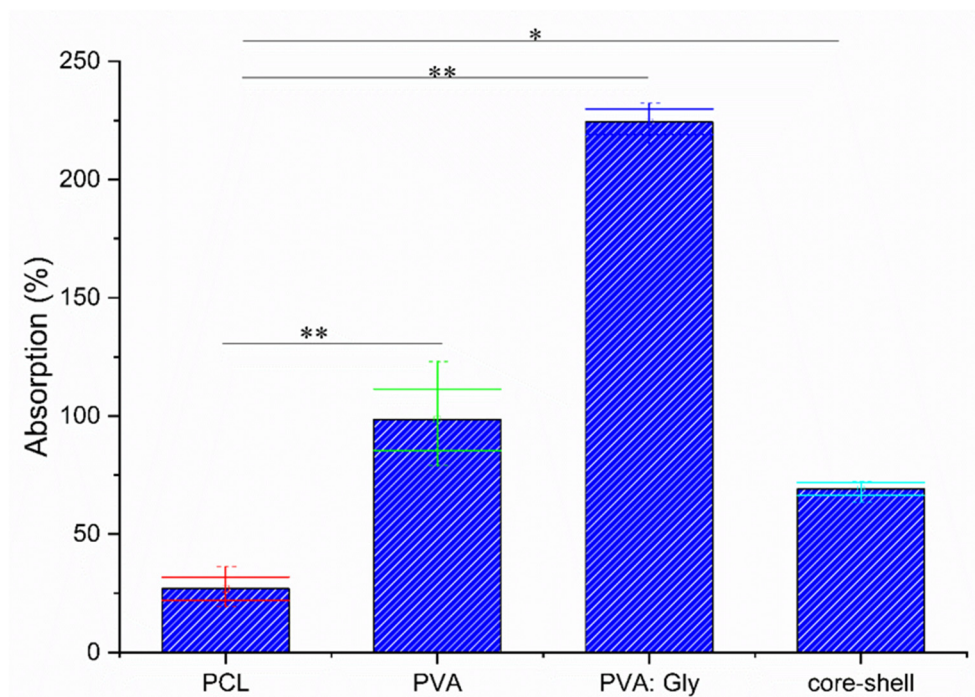


Figure 9. Absorption % of the PCL, PVA, PVA:Gly, and core-shell membranes. All readings are presented as remaining weight% \pm SD. ANOVA; ** $p < 0.001$ and * $p < 0.01$.

4. Discussion

The fibrous structure, which mimics ECM, is essential for cells attachment, proliferation, differentiation, and infiltration. On the other hand, the fiber diameter and pore size are critical parameters in tissue regeneration application. For instance, scaffolds with a pore size less than 1 μm improve cell-surface interaction, while a larger pore size 1–3 μm is necessary for cell-to-cell communication, and a 3–12 μm pore size is suitable for cell migration and proliferation [26]. Furthermore, a pore size between 50–150 μm is essential for bone cell infiltration [27], and 50 μm for dermal fibroblasts infiltration. Even though the suitable pore size for GBR membrane is still controversial between studies and no optimal pore size has been confirmed yet, the interconnected microporous structure with a pore size between 0.2 and 500 μm is most commonly used commercially [28].

Moreover, the core solvent in the fabricated core-shell membrane was pure water, while the shell solvents were chloroform and methanol. Due to the miscibility of methanol in water, there was no defined line between the core structure and the shell structure, as demonstrated in Figure 4a [29]. Moreover, pure water was the solvent for PVA and Gly in PVA, PVA:Gly, and core in core-shell membranes; however, due to high surface tension of water, Triton X-100 was added to the solution as a surfactant to lower solution surface tension and enhance the formation of bead-less fibers. Since all the fabricated membranes exhibited nano-scale fibers diameter and micro-scale pore size, they are suitable for GBR application. That is due to the enhancement of bone regeneration and restriction of fibroblasts and other fast-growing cells infiltration.

The core structure was fully encapsulated with the shell structure (as shown in Figure 4); however, the shell structure was very thin in comparison to the thick core. The reason for this is that the feeding rate of the core was much higher than the shell's feeding rate. On the other hand, the needle-like shape of the Gly inside the fiber (as shown in Figure 4b), according to Ferrari et al., is a β -glycine [30]. Moreover, Bai et al. demonstrated the needle-like shape of the β -glycine using optical microscopy [31].

The modulus of elasticity is an indication of the membrane resistance to elastic deformation; according to the modulus of elasticity results, the stiffest membrane is the PVA:Gly, while the PCL has the lowest modulus elasticity among other membranes. The low modulus of elasticity is an indication of proneness to tearing and difficulty in handling the membrane. Therefore, the core-shell membrane has a moderate average modulus of elasticity of 135.3 ± 3.05 MPa, which is suitable for GBR membrane application. On the other hand, the average UTS of the core-shell membrane, which equals 4.57 ± 0.04 MPa, was significantly higher than the UTS of the PCL and the PVA membranes ($p < 0.05$). In comparison with commercially used GBR membranes, including Bio-Gide and Ossix Plus dry UTS, the core-shell membrane UTS did not show any significant difference ($p < 0.05$) [32]. Regarding average elongation at break, fabricated membranes revealed significantly different values, with the highest value for the electrospun PCL and a moderate value (~40%) for the core-shell membrane.

In addition to that, it should be noted that adding the Gly into the PVA membrane significantly enhanced the mechanical properties of the membrane, and that is one of the advantages of Gly inclusion. Furthermore, the fabricated core-shell membrane shows a moderate average modulus of elasticity, UTS, and elongation at break in the benefits of the core PVA:Gly strength and the shell PCL elasticity.

In high-resolution scans of O_{1s} , C_{1s} , and N_{1s} , since both PCL and PVA contain only oxygen and carbon atoms, their high-resolution spectrum of N_{1s} exhibited the absence of the N_{1s} peak. Additionally, the core-shell membrane shows no N_{1s} characteristic peak, which is due to the full encapsulation of the core by the shell material. Only the PVA:Gly membrane exhibited the presence of N_{1s} peak at 400 eV, which was assigned to the C-NH₂ bond.

Moreover, in the PCL membrane, C_{1s} high-resolution spectrum peaks at 285, 286.4, and 289 eV are attributed to the C-C, C-O, and C=O, respectively. In the core-shell membrane, the same C_{1s} peaks as the PCL membrane were found; however, with less chemical composition. On the other hand, the O_{1s} high-resolution spectrum of the PCL and core-shell membranes peaks were at 531 and 533 eV and corresponds to the C=O bond and C-O bonds, respectively. The existence of the same C_{1s} and O_{1s} peaks in both the PCL membrane and core-shell membrane are an indication of the PCL chemical composition on the surface of the core-shell membrane and fully encapsulation of the PVA core. However, the C_{1s} and O_{1s} peak intensities were different in both membranes, with lower C_{1s} and higher O_{1s} peaks in the core-shell, which is an indication of the existence of more hydrophilic PCL in the core-shell membrane [33]. This is assumed to be due to some degree of interaction between the carboxyl and hydroxyl groups in PCL and PVA, respectively.

In PVA and PVA:Gly membranes, the C_{1s} peaks were found to be 285 and 286 eV and that they represent the C-C and C-O bonds, respectively, while the O_{1s} peak was found to be 533 eV and that was assigned to the C-O bond. The peaks' intensities were the same in both membranes except for N_{1s} peak at 400 eV in the PVA:Gly, which is an indication of the Gly inclusion in the electrospun membrane.

The main originality in this paper is using the Gly in its β crystallographic conformation form due to its mechanical and piezoelectric properties, which support bone cells formation [34]. Similar to the XPS analysis, XRD was used to investigate the material's chemical structure, although the main difference between XPS and XRD is that XRD is used to determine the crystallographic structure based on the diffraction of X-rays. Therefore, the XRD analysis was used to identify the β -Gly form in the PVA:Gly and core-shell membranes. The XRD pattern of the core-shell and PVA:Gly membranes revealed a very

wide peak in the range of 7–25°, which is an indication of the amorphous structure of PVA due to the absence of well-defined and intensive Bragg diffraction peak [35]. The amorphous structure of the PVA in both fibrous structures was caused by the destruction of the orientation order of the PVA chains and even by the formation of amorphous bond layers around the Gly crystals [36].

Commonly reported in the literature, the 2 θ diffraction peaks that equal nearly 18°, 24°, and 28° belong to the (001), (110), and (020) β -Gly crystallographic configuration, respectively [30,31,37–39]. Moreover, Es et al. [18] fabricated a glycine-chitosan flexible biodegradable sensor that shows high piezoelectric properties, and the evaluated XRD confirmed the formation of the same Gly diffraction peaks found in this paper. On the other hand, the core-shell membrane XRD pattern showed the same diffraction peaks as the PVA:Gly membrane except for the sharp peak that equals 21.5°. This sharp peak represents the (110) crystallographic configuration of semi-crystalline PCL according to the literature [40].

The TGA was used to specify the changes in membrane composition and thermal stability of each fabricated membrane. The electrospun PCL membrane showed a one-step decomposition with a single temperature. The one-step thermal degradation started at 190 °C and ended up at around 460 °C; furthermore, the electrospun PCL lost 95% of its weight at around 398 °C, which was comparable to another study [41].

On the other hand, the PVA electrospun membrane exhibited three weight-loss regions, which are: ~240, ~355, and ~429 °C; during each one, the PVA lost 44.2%, 22.5%, and 21.65% of its weight, respectively. The first weight loss region is due to the elimination of water molecules trapped in the membrane, while the second and the third are due to the elimination of the side group and the breakdown of the PVA polymer backbone, respectively.

While the PVA:Gly membrane TGA plot showed a different thermal decomposition curve with two weight loss regions at ~238 and ~319 °C, in which it lost 7.2% and 81.4% of weight, respectively, the first weight loss region is believed to be due to the decomposition of Gly crystals, as claimed in the literature [42]. Furthermore, the decomposition of PVA was about 319 °C with a one-step thermal decomposition process. On the other hand, the core-shell showed the same Gly thermal decomposition step at ~238 °C, in which it lost 8.14% of its weight, while the rest of the complex structure appeared in a one-step decomposition at about 355 °C in which 84% of the mass was lost. Therefore, the thermal stability of the core-shell in comparison to PVA:Gly membrane was enhanced due to the addition of PCL as a shell material or the complex structure of the core-shell. However, the four fabricated membranes exhibit good thermal stability with a maximum decomposition temperature of around 350 °C.

Generally, cells adhere to moderately hydrophilic surfaces; therefore, in scaffold fabrication, many surface modification techniques are applied to hydrophobic surfaces, such as plasma treatment [43]. The PCL fabricated membrane showed a hydrophobic surface with an average C.A of almost 100°. On the contrary, the PVA and the PVA:Gly membranes revealed a tremendously flat hydrophilic C.A, which was unable to be captured by the camera; therefore, we considered it as almost zero. However, the core-shell membrane showed a significant enhancement in the C.A with $47.4 \pm 2.2^\circ$, which is considered a hydrophilic surface. According to the literature, a 50° C.A value is considered as the most suitable contact angle for cell adhesion since it is the C.A of the commercial tissue culture polystyrene (TCPS). Therefore, a moderately hydrophilic membrane that is highly favored for cell attachment and proliferation was successfully developed.

Furthermore, the PCL membrane demonstrated a low degradation rate with an average weight remaining of $90.2\% \pm 2.2\%$ after 90 days of incubation in PBS. On the other hand, the PVA and PVA:Gly membranes showed a significantly high degradation rate with an average remaining weight percentage of $11.07\% \pm 2.6\%$ and $17.28\% \pm 1.78\%$, respectively, after 90 days of incubation. However, the core-shell membrane revealed a moderate degradation rate after 90 days of incubation with $45.57\% \pm 1.68\%$ of the weight

remaining. This result reflects the effectiveness of the coaxial electrospinning technique to fabricate the core-shell structure membrane to overcome the cross-linking process of the highly degradable membranes. In addition to that, the core-shell nanofibrous structure according to moderate degradation rate is a good candidate for GBR application since the prolonged biodegradation is associated with decreased tissue attachment, proliferation, vascularization, and foreign body reaction [44]. On the other hand, a shortened biodegradation rate hinders the effectiveness of the GBR membrane.

Regarding absorption of the fabricated membranes, the PCL membrane, which showed high hydrophobicity, exhibited a significantly low absorption of $26.9 \pm 1.62\%$. On the other hand, the PVA membrane, which exhibited a high hydrophilicity, showed a significant difference in comparison with the PCL membrane in average absorption with an almost 100% increment. An extremely significant increase was found in PVA:Gly membrane absorption with an almost 225% increase in weight compared to PVA and PCL membranes. We claim that the significant difference between PVA and PVA:Gly is due to the amorphous structure of the PVA in the PVA:Gly membrane, which was caused by the destruction of the orientation order of the PVA chains by the formation of an amorphous bond layer around the Gly crystals, and this is the same results found in XRD analysis. While the core-shell membrane showed a moderate absorption equal to $69.09 \pm 2.7\%$ in comparison to PCL and PVA:Gly membranes, and no significant difference compared to PVA membrane. In this respect, the absorption capacity represents the material supporting the humid environment that is responsible for the transportation of constituents of body fluids to the injury site during the regeneration process. Therefore, moderate absorption is favored in tissue regeneration applications, which is compensation of neither volume change due to high absorption nor reduction of body fluid nutrients and oxygen contribution.

On the other hand, the PVA and PVA:Gly showed a high shrinkage % due to extremely high hydrophilicity; therefore, the membranes swelled, aggregated, and lost their shape, the core shell showed a significantly lower average shrinkage % in comparison to PVA and PVA:Gly. That is due to the shell PCL structure, which preserves the core structure from contact with its surrounding; therefore, no significant change in volume was observed. However, we should notice the moderate absorption % even though the shell layer resists water absorption. The reason for that is the high surface area to volume and high porosity of the electrospun membrane that allows the water to be trapped between the nanofibers rather than being absorbed, which causes no volume change.

5. Conclusions

In this paper, a core-shell nanofibrous membrane, in which the Gly and PVA is the core and PCL is the shell, was coaxially electrospun in order to improve the mechanical, physical, and chemical properties of the monolithic electrospun membranes. For instance, The PVA and PVA:Gly membranes had an extremely high hydrophilicity and degradation rate, and therefore, require a cross-linking process. On the other hand, PCL exhibited a hydrophobic structure with a long degradation rate and unsuitable mechanical properties. Therefore, the core-shell membrane, with PCL as the shell material and PVA:Gly as the core material, is suggested as a membrane for GBR application. The encapsulation of the Gly and PVA core with a PCL shell and the nanofibers and interconnected micropores overcame the drawbacks of the core and the shell materials individually and produced a membrane with the advantages of both materials.

For instance, the mechanical properties, including modulus of elasticity, UTS, and elongation to break, were improved in comparison to PVA and PCL electrospun membranes with 135 ± 3.05 MPa, 4.57 ± 0.04 MPa, and $39.43\% \pm 0.58\%$, respectively. Furthermore, the TEM and XRD results of 18° , 24° and 28° Bragg peaks prove the existence of the Gly in β form. While the core-shell membrane wettability of $47.4 \pm 2.2^\circ$, C.A is much more suitable for GBR applications in comparison with the other fabricated membranes.

Author Contributions: Conceptualization, writing, editing, and investigation, M.A.; supervision and reviewing, N.K.A.A.; conceptualization, supervision, and reviewing H.T.S. All authors have read and agreed to the published version of the manuscript.

Funding: This research received no external funding.

Institutional Review Board Statement: Not applicable.

Informed Consent Statement: Not applicable.

Conflicts of Interest: The authors declare no conflict of interest.

References

1. Pina, S.; Ribeiro, V.P.; Marques, C.F.; Maia, F.R.; Silva, T.H.; Reis, R.L.; Oliveira, J.M. Scaffolding strategies for tissue engineering and regenerative medicine applications. *Materials* **2019**, *12*, 1824. [\[CrossRef\]](#)
2. Gozutok, M.; Basar, A.O.; Sasmazel, H.T. Development of Antibacterial Composite Electrospun Chitosan-Coated Polypropylene Materials. *J. Nanosci. Nanotechnol.* **2018**, *18*, 2881–2891. [\[CrossRef\]](#)
3. Laney, W.R. Glossary of Oral and Maxillofacial Implants. *Int. J. Oral Maxillofac. Implant.* **2017**, *32*. [\[CrossRef\]](#)
4. Zupancic, S.; Kocbek, P.; Baumgartner, S.; Kristl, J. Contribution of Nanotechnology to Improved Treatment of Periodontal Disease. *Curr. Pharm. Des.* **2015**, *21*, 3257–3271. [\[CrossRef\]](#)
5. Basar, A.O.; Sadhu, V.; Turkoglu Sasmazel, H. Preparation of Electrospun PCL-Based Scaffolds by Mono/Multi-Functionalized GO. *Biomed. Mater.* **2019**, *14*, 045012. [\[CrossRef\]](#) [\[PubMed\]](#)
6. Surucu, S.; Sasmazel, H.T. DBD Atmospheric Plasma-Modified, Electrospun, Layer-by-Layer Polymeric Scaffolds for L929 Fibroblast Cell Cultivation. *J. Biomater. Sci. Polym. Ed.* **2016**, *27*, 111–132. [\[CrossRef\]](#) [\[PubMed\]](#)
7. Sasmazel, H.T. Novel Hybrid Scaffolds for the Cultivation of Osteoblast Cells. *Int. J. Biol. Macromol.* **2011**, *49*, 838–846. [\[CrossRef\]](#)
8. Bružauskaitė, I.; Bironaitė, D.; Bagdonas, E.; Bernotiene, E. Scaffolds and Cells for Tissue Regeneration: Different Scaffold Pore Sizes—Different Cell Effects. *Cytotechnology* **2015**, *68*, 355–369. [\[CrossRef\]](#) [\[PubMed\]](#)
9. Surucu, S.; Turkoglu Sasmazel, H. Development of Core-Shell Coaxially Electrospun Composite PCL/Chitosan Scaffolds. *Int. J. Biol. Macromol.* **2016**, *92*, 321–328. [\[CrossRef\]](#) [\[PubMed\]](#)
10. Ozkan, O.; Sasmazel, H.T. Antibacterial Performance of PCL-Chitosan Core-Shell Scaffolds. *J. Nanosci. Nanotechnol.* **2018**, *18*, 2415–2421. [\[CrossRef\]](#)
11. Soldatos, N.K.; Stylianou, P.; Koidou, V.P.; Angelov, N.; Yukna, R.; Romanos, G.E. Limitations and Options Using Resorbable versus Nonresorbable Membranes for Successful Guided Bone Regeneration. *Quintessence Int.* **2017**, *48*, 131–147. [\[CrossRef\]](#)
12. Toledano, M.; Gutierrez-Pérez, J.L.; Gutierrez-Corrales, A.; Serrera-Figallo, M.A.; Toledano-Orsorio, M.; Rosales-Leal, J.I.; Aguilar, M.; Osorio, R.; Torres-Lagares, D. Novel Non-Resorbable Polymeric-Nanostructured Scaffolds for Guided Bone Regeneration. *Clin. Oral. Investig.* **2020**, *24*, 2037–2049. [\[CrossRef\]](#)
13. Gentile, P.; Chiono, V.; Tonda-Turo, C.; Ferreira, A.M.; Ciardelli, G. Polymeric Membranes for Guided Bone Regeneration. *Biotechnol. J.* **2011**, *6*, 1187–1197. [\[CrossRef\]](#) [\[PubMed\]](#)
14. Wang, J.; Wang, L.; Zhou, Z.; Lai, H.; Xu, P.; Liao, L.; Wei, J. Biodegradable Polymer Membranes Applied in Guided Bone/Tissue Regeneration: A Review. *Polymer* **2016**, *8*, 115. [\[CrossRef\]](#)
15. Zhong, Z.; Wheeler, M.D.; Li, X.; Froh, M.; Schemmer, P.; Yin, M.; Bunzendaul, H.; Bradford, B.; Lemasters, J.J. L-Glycine: A Novel Antiinflammatory, Immunomodulatory, and Cytoprotective Agent. *Curr. Opin. Clin. Nutr. Metab. Care* **2003**, *6*, 229–240. [\[CrossRef\]](#) [\[PubMed\]](#)
16. Wang, W.; Wu, Z.; Dai, Z.; Yang, Y.; Wang, J.; Wu, G. Glycine Metabolism in Animals and Humans: Implications for Nutrition and Health. *Amino Acids* **2013**, *45*, 463–477. [\[CrossRef\]](#)
17. Guerin, S.; Stapleton, A.; Chovan, D.; Mouras, R.; Gleeson, M.; Mckeown, C.; Noor, M.; Silien, C.; Rhen, F.; Kholkin, A.; et al. Control of Piezoelectricity in Amino Acids by Supramolecular Packing. *Nat. Mater.* **2018**, *17*, 180–186. [\[CrossRef\]](#)
18. Hosseini, E.S.; Manjakkal, L.; Shakhivel, D.; Dahiya, R. Glycine-Chitosan-Based Flexible Biodegradable Piezoelectric Pressure Sensor. *ACS Appl. Mater. Interfaces* **2020**, *12*, 9008–9016. [\[CrossRef\]](#) [\[PubMed\]](#)
19. Hosseini, E.S.; Dahiya, R. Biodegradable Amino Acid-Based Pressure Sensor. In Proceedings of the 2020 IEEE Sensors, online, 25–28 October 2020; pp. 1–4.
20. Hosseini, E.S.; Manjakkal, L.; Shakhivel, D.; Dahiya, R. Glycine-Based Flexible Biocompatible Piezoelectric Pressure Sensor for Healthcare Applications. In Proceedings of the 2020 IEEE International Conference on Flexible and Printable Sensors and Systems (FLEPS), Manchester, UK, 16–19 August 2020; pp. 1–4.
21. Mohamed, R.M.; Yusoh, K. A Review on the Recent Research of Polycaprolactone (PCL). *Adv. Mater. Res.* **2016**, *1134*, 249–255. [\[CrossRef\]](#)
22. Gozutok, M.; Sadhu, V.; Sasmazel, H.T. Development of Poly(Vinyl Alcohol) (PVA)/Reduced Graphene Oxide (RGO) Electrospun Mats. *J. Nanosci. Nanotechnol.* **2019**, *19*, 4292–4298. [\[CrossRef\]](#)
23. Elgali, I.; Omar, O.; Dahlin, C.; Thomsen, P. Guided Bone Regeneration: Materials and Biological Mechanisms Revisited. *Eur. J. Oral Sci.* **2017**, *125*, 315–337. [\[CrossRef\]](#) [\[PubMed\]](#)

24. Arakawa, C.K.; DeForest, C.A. Chapter 19—Polymer Design and Development. In *Biology and Engineering of Stem Cell Niches*; Vishwakarma, A., Karp, J.M., Eds.; Academic Press: Boston, MA, USA, 2017; pp. 295–314. ISBN 978-0-12-802734-9.
25. Alhosseini, S.; Moztarzadeh, F.; Mozafari, M.; Asgari, S.; Dodel, M.; Samadikuchaksaraei, A.; Kargozar, S.; Jalali, N. Synthesis and Characterization of Electrospun Polyvinyl Alcohol Nanofibrous Scaffolds Modified by Blending with Chitosan for Neural Tissue Engineering. *Int. J. Nanomed.* **2012**, *7*, 25–34. [[CrossRef](#)]
26. Mc, P.; Wc, C.; Jm, G.; Ga, C.; Sl, B. Increasing the Pore Sizes of Bone-Mimetic Electrospun Scaffolds Comprised of Polycaprolactone, Collagen I and Hydroxyapatite to Enhance Cell Infiltration. *Biomaterials* **2011**, *33*, 524–534. [[CrossRef](#)]
27. Wang, X.; Lou, T.; Zhao, W.; Song, G.; Li, C.; Cui, G. The Effect of Fiber Size and Pore Size on Cell Proliferation and Infiltration in PLLA Scaffolds on Bone Tissue Engineering. *J. Biomater. Appl.* **2016**, *30*, 1545–1551. [[CrossRef](#)]
28. de Santana, R.B.; de Mattos, C.M.L.; Francischone, C.E.; Van Dyke, T. Superficial Topography and Porosity of an Absorbable Barrier Membrane Impacts Soft Tissue Response in Guided Bone Regeneration. *J. Periodontol.* **2010**, *81*, 926–933. [[CrossRef](#)] [[PubMed](#)]
29. Han, D.; Steckl, A. Coaxial Electrospinning Formation of Complex Polymer Fibers and Their Applications. *ChemPlusChem* **2019**, *84*, 1451. [[CrossRef](#)]
30. Ferrari, E.S.; Davey, R.J.; Cross, W.I.; Gillon, A.L.; Towler, C.S. Crystallization in Polymorphic Systems: The Solution-Mediated Transformation of β to α Glycine. *Cryst. Growth Des.* **2003**, *3*, 53–60. [[CrossRef](#)]
31. Bai, C.; Wang, C.; Tengfei, Z.; Hu, Q. Growth of β -Glycine Crystals Promoted by Standing Surface Acoustic Waves (SSAWs). *CrystEngComm* **2018**, *20*, 1245–1251. [[CrossRef](#)]
32. Raz, P.; Brosh, T.; Ronen, G.; Tal, H. Tensile Properties of Three Selected Collagen Membranes. *BioMed Res. Int.* **2019**, 2019. [[CrossRef](#)]
33. Cho, S.J.; Jung, S.M.; Kang, M.; Shin, H.S.; Youk, J.H. Preparation of Hydrophilic PCL Nanofiber Scaffolds via Electrospinning of PCL/PVP-b-PCL Block Copolymers for Enhanced Cell Biocompatibility. *Polymer* **2015**, *69*, 95–102. [[CrossRef](#)]
34. Kim, D.; Han, S.A.; Kim, J.H.; Lee, J.-H.; Kim, S.-W.; Lee, S.-W. Biomolecular Piezoelectric Materials: From Amino Acids to Living Tissues. *Adv. Mater.* **2020**, *32*, 1906989. [[CrossRef](#)]
35. Reddy, M.O.; Chandra Babu, B. Structural, Optical, Electrical, and Magnetic Properties of PVA:Gd³⁺ and PVA:Ho³⁺ Polymer Films. *Indian J. Mater. Sci.* **2015**, 2015, e927364. [[CrossRef](#)]
36. Bang, H.; Watanabe, K.; Nakashima, R.; Kai, W.; Song, K.-H.; Lee, J.S.; Gopiraman, M.; Kim, I.-S. A Highly Hydrophilic Water-Insoluble Nanofiber Composite as an Efficient and Easily-Handleable Adsorbent for the Rapid Adsorption of Cesium from Radioactive Wastewater. *RSC Adv.* **2014**, *4*, 59571–59578. [[CrossRef](#)]
37. Tamura, H.; Kadota, K.; Shirakawa, Y.; Tozuka, Y.; Shimosaka, A.; Hidaka, J. Morphology Control of Amino Acid Particles in Interfacial Crystallization Using Inkjet Nozzle. *Adv. Powder Technol.* **2014**, *25*, 847–852. [[CrossRef](#)]
38. Ouyang, L.; Zheng, T.; Shen, L. Direct Observation of α - to β -Glycine Transformation during the Ionic Liquid-Mediated Crystallization Process. *CrystEngComm* **2018**, *20*, 2705–2712. [[CrossRef](#)]
39. Isakov, D.; Gomes, E.d.M.; Bdikin, I.; Almeida, B.; Belsley, M.; Costa, M.; Rodrigues, V.; Heredia, A. Production of Polar β -Glycine Nanofibers with Enhanced Nonlinear Optical and Piezoelectric Properties. *Cryst. Growth Des.* **2011**, *11*, 4288–4291. [[CrossRef](#)]
40. Wang, X.; Zhao, H.; Turng, L.-S.; Li, Q. Crystalline Morphology of Electrospun Poly(ϵ -Caprolactone) (PCL) Nanofibers. *Ind. Eng. Chem. Res.* **2013**, *52*, 4939–4949. [[CrossRef](#)]
41. Sayyar, S.; Murray, E.; Thompson, B.C.; Gambhir, S.; Officer, D.L.; Wallace, G.G. Covalently Linked Biocompatible Graphene/Polycaprolactone Composites for Tissue Engineering. *Carbon* **2013**, *52*, 296–304. [[CrossRef](#)]
42. Weiss, I.M.; Muth, C.; Drumm, R.; Kirchner, H.O.K. Thermal Decomposition of the Amino Acids Glycine, Cysteine, Aspartic Acid, Asparagine, Glutamic Acid, Glutamine, Arginine and Histidine. *BMC Biophys* **2018**, *11*, 2. [[CrossRef](#)]
43. Turkoglu Sasmazel, H.; Alazzawi, M.; Kadim Abid Alsahib, N. Atmospheric Pressure Plasma Surface Treatment of Polymers and Influence on Cell Cultivation. *Molecules* **2021**, *26*, 1665. [[CrossRef](#)]
44. Rothamel, D.; Schwarz, F.; Sager, M.; Herten, M.; Sculean, A.; Becker, J. Biodegradation of Differently Cross-Linked Collagen Membranes: An Experimental Study in the Rat. *Clin. Oral Implant. Res.* **2005**, *16*, 369–378. [[CrossRef](#)] [[PubMed](#)]